Simulation of Three Material Partial Volume Averaging in a Software Breast Phantom

Feiyu Chen[1], David D. Pokrajac[1], Xiquan Shi[1], Fengshan Liu[1], Andrew D.A. Maidment[2], and Predrag R. Bakic[2]

[1] Delaware State University, 1200 N DuPont Hwy, Dover DE 19904
FChen09@students.desu.edu,{DPokrajac,XShi,FLiu}@desu.edu
[2] University of Pennsylvania, 3400 Spruce Street, Philadelphia, PA 19104
{Predrag.Bakic,Andrew.Maidment}@uphs.upenn.edu

Abstract. A general case for simulation of partial volume (PV) averaging in software breast phantoms is presented. PV simulation could improve the quality of phantom images by reducing quantization artifacts near borders between different materials. The validity of phantom studies depends on the realism of simulated images, which is affected by the size of phantom voxels. Large voxels may cause notable quantization artifacts; small voxels, however, extend the generation time and increase the memory requirements. An improvement in image quality without reducing voxel size is achievable by the simulation of PV averaging in voxels containing more than one simulated tissue type; the linear x-ray attenuation coefficient of such voxels is represented by a combination of attenuation coefficients proportional to voxel subvolumes occupied by different tissues. In this paper, we present results of simulated PV in the general case of voxels containing up to three materials.

Keywords: Digital mammography, computer breast phantom, partial volume simulation, computational geometry.

1 Introduction

This study is motivated by the desire to improve the quality of synthetic images generated using software breast phantoms. The partial volume (PV) averaging can help reduce the quantization artifacts on boundaries of regions with different simulated materials. The software phantoms in this study have been generated based upon the recursive partitioning of the phantom volume using octrees [1]. In this paper, we propose a solution for a general PV case with up to three simulated materials in a voxel. This work represents the first PV simulation in software phantoms generated based upon the rules for simulating anatomical structures [1-4]. PV simulation has been indirectly reported in a method for generating phantoms based upon the CT images of mastectomy specimen [5]. In that method, the values of each reconstructed breast CT image voxel were scaled and interpreted as the percentage of adipose breast tissue in the voxel.

A.D.A. Maidment, P.R. Bakic, and S. Gavenonis (Eds.): IWDM 2012, LNCS 7361, pp. 149–156, 2012.

In this paper, we present an overview of the PV simulation method including details of a planar approximation and the PV computation. The improvement of image quality is qualitatively validated. The results are shown in the form of slices and simulated X-ray projections of phantoms with and without PV.

2 Method

The effective linear x-ray attenuation in a voxel which contains more than one simulated material can be calculated as:

$$\mu_V = \frac{1}{|V|}\sum_i \mu_i |V_i| = \sum_i \mu_i p_i \; ; \; p_i = \frac{|V_i|}{|V|} \times 100\% \, , \tag{1}$$

where $|V|$ is the voxel volume, $|V_i|$ is the subvolume of material i with the linear x-ray attenuation μ_i, and p_i is the percentage of the material i in the voxel (Fig. 1a). One can distinguish the following cases of PV (Fig 1b):

A. *Two materials with one bounding surface*: (1) Skin and air; (2) Cooper's ligament and adipose tissue; (3) Ligament and fibroglandular dense tissue; (4) Skin and dense tissue; (5) Skin and adipose tissue, and (6) Skin and Cooper's ligament;
B. *Three materials with two bounding surfaces*: (7) Skin, ligament, and dense tissue; and (8) Skin, ligament, and adipose tissue

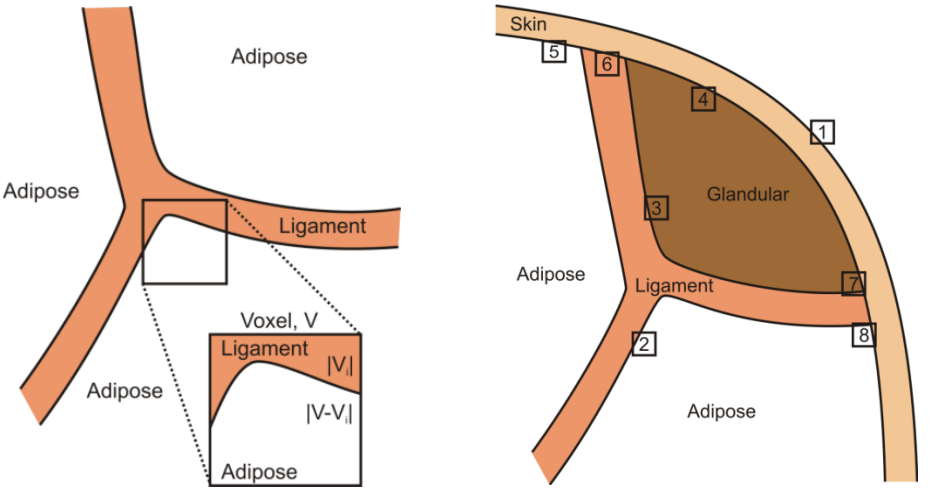

Fig. 1. (a) The concept of PV simulation; V denotes the voxel volume and V_i is the sub-volume occupied by dense tissue.(b) Different cases of material combination in a voxel.

The simulation of PV case (1) has been reported previously [6]; it can be easily extended to cases (2)-(6). In this abstract we present a general case of PV simulation based upon the planar approximation of up to two bounding surfaces in a voxel, addressing cases (7)-(8).

The planar approximation for the boundary between Cooper's ligaments and adipose tissue, as simulated in our software breast phantom [1], can be obtained as follows. Adipose compartments C_i and C_j, which may be given by shape functions f_i and f_j, determine a Cooper's ligament between them as the locus of points within a distance of D/2 from a surface $F_{ij}(\mathbf{x})= f_i(\mathbf{x})- f_j(\mathbf{x})$, see Fig. 2. Consider a voxel V with center $\mathbf{x}_c$. We define a planar approximation π_1 of the boundary between the Cooper's ligament and the compartment C_j as

$$\pi_1 : (\mathbf{x}-\mathbf{x}_1)\cdot sign\left(F_{ij}(\mathbf{x}_c)\right)\nabla F_{ij}(\mathbf{x}_c)=0, \tag{2}$$

where

$$\mathbf{x}_1 = \mathbf{x}_c + sign\left(F_{ij}(\mathbf{x}_c)\right)\left(\mathrm{D}/2-\frac{F_{ij}(\mathbf{x}_c)}{\left\|\nabla F_{ij}(\mathbf{x}_c)\right\|}\right)\frac{\nabla F_{ij}(\mathbf{x}_c)}{\left\|\nabla F_{ij}(\mathbf{x}_c)\right\|}. \tag{3}$$

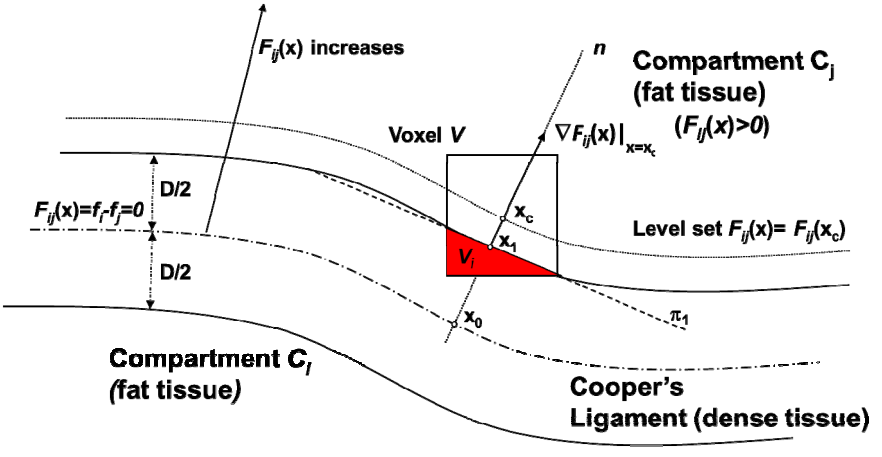

Fig. 2. Planar approximation of a boundary between Cooper's ligament and a compartment

In a general PV case with three simulated materials and two bounding surfaces in a voxel, we can construct a planar approximation for each bounding surface (Fig. 3). The result of the approximation are planes $\pi_1 : (\mathbf{x}-\mathbf{x}_1)\hat{\mathbf{n}}_1 = 0$ and $\pi_2 : (\mathbf{x}-\mathbf{x}_2)\hat{\mathbf{n}}_1 = 0$. The partial volumes $|V_i|$ of interest are subsequently calculated as the volume of a portion of the voxel V (with center $\mathbf{x}_c$) that is bellow/above the planes. For example, the PV V_i corresponding to the fat tissue in Figure 4 is computed as a volume of a part of the voxel that is both above planes π_1 and π_2.

The PV V_i in a voxel shown in Fig. 3 has been computed using planar approximations as follows. Consider a voxel of linear size Δx, with a vertex **v** located above planes π_1 and π_2. (If no such vertex exists, the PV should be zero).

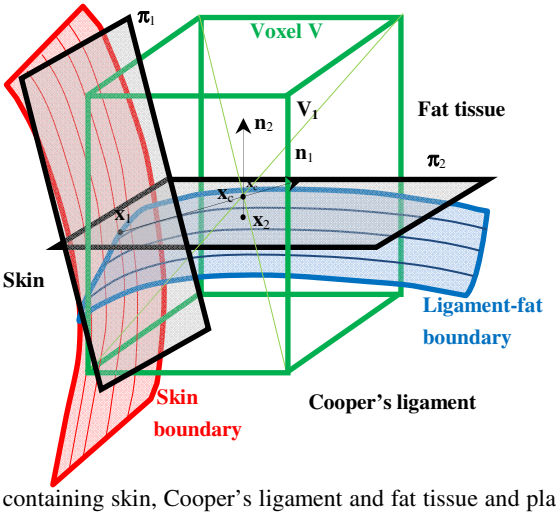

Fig. 3. A voxel containing skin, Cooper's ligament and fat tissue and planar approximations π_1 and π_2 of the tissue boundaries

The divergence (or Gauss-Ostrogradsky) theorem [7] is employed to compute the partial volume $|V_i|$ of the voxel above planes π_1 and π_2, where the volume V_i is bounded by planes π_1 and π_2 and at most 6 sides of the voxel. The divergence theorem can be described as the following integral equation:

$$\iiint_{V_i} (\nabla \cdot F) dV = \oiint_S (F \cdot \mathbf{n}) dS \,. \tag{4}$$

The left side is a volume integral over the partial volume V_i of voxel, the right side is the surface integral over the boundary of the volume V_i, and n is the outward pointing unit normal vector of the boundary.

After the appropriate choice of the vector field function inside the integral at left side, *i.e.,* $F(\mathbf{x}) = \mathbf{x}$, the whole quantity at the left side becomes $3|V_i|$, and the right side can be rewritten as:

$$\left(S_1 + S_2 + S_3\right)\Delta x + A_{\pi 1} d_1 + A_{\pi 2} d_2 \,, \tag{5}$$

where S_i, i=1,3 are surface areas of the boundary formed by the voxel sides σ_1 ,σ_2 and σ_3, that do not contain the vertex **v**; $A_{\pi 1}$ and $A_{\pi 2}$ are surface areas of the boundary of V_i belonging to planes π_1 and π_2.

Subsequently, the PV can be calculated as:

$$|V_i| = \frac{(S_1 + S_2 + S_3)\Delta x + A_{\pi 1} d_1 + A_{\pi 2} d_2}{3}, \tag{6}$$

where $d_1 = (\mathbf{v} - \mathbf{x}_1)\hat{\mathbf{n}}_1$, and $d_2 = (\mathbf{v} - \mathbf{x}_2)\hat{\mathbf{n}}_2$ are distances of the vertex **v** to planes π_1 and π_2.

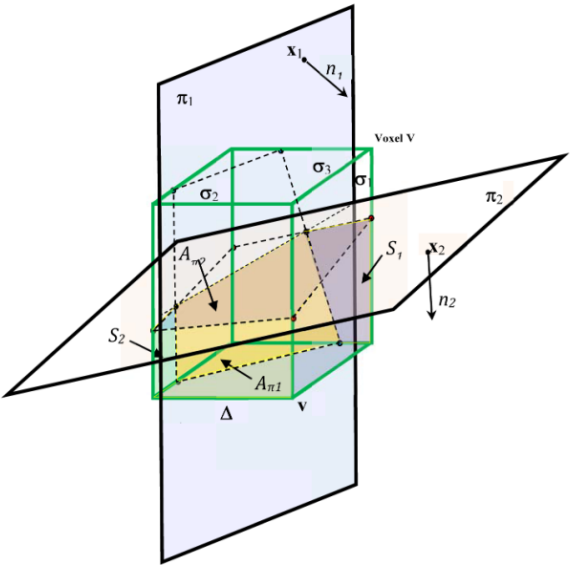

Fig. 4. Partial volume V_i of the voxel V above planes π_1 and π_2 and containing vertex **v**. S_1, S_2 and S_3(here S_3=0) are surface areas of parts of the volume boundary belonging to voxel sides σ_1, σ_2 and σ_3 that do not contain the vertex **v**.

3 Results and Discussion

Fig. 5 illustrates the PV simulation in a 450ml software breast phantom with 400μm voxels. Shown is the segmentation of phantom detail into air and voxels containing one, two or three materials. For the corresponding phantom detail, shown also are the equivalent linear x-ray attenuations, and percentages of ligament tissue and skin tissue.

Fig. 5 suggests that the PV simulation on the ligaments-fat boundary was qualitatively correct. The voxels containing two materials are detected at the boundaries of two materials (e.g., skin, compartment). Similarly, the three material voxels are detected where the skin meets Cooper's ligaments and a compartment. Fig. 5b indicates that the PV helped smooth the appearance of boundaries between regions with different x-ray attenuations. The computed percentages of ligament and skin tissues in a voxel (Figs. 5c, 5d) suggest the correctness of the applied algorithm. The voxels in the interior of skin/ligaments contain 100% of the corresponding tissues, while the percentages gradually decrease at the boundaries.

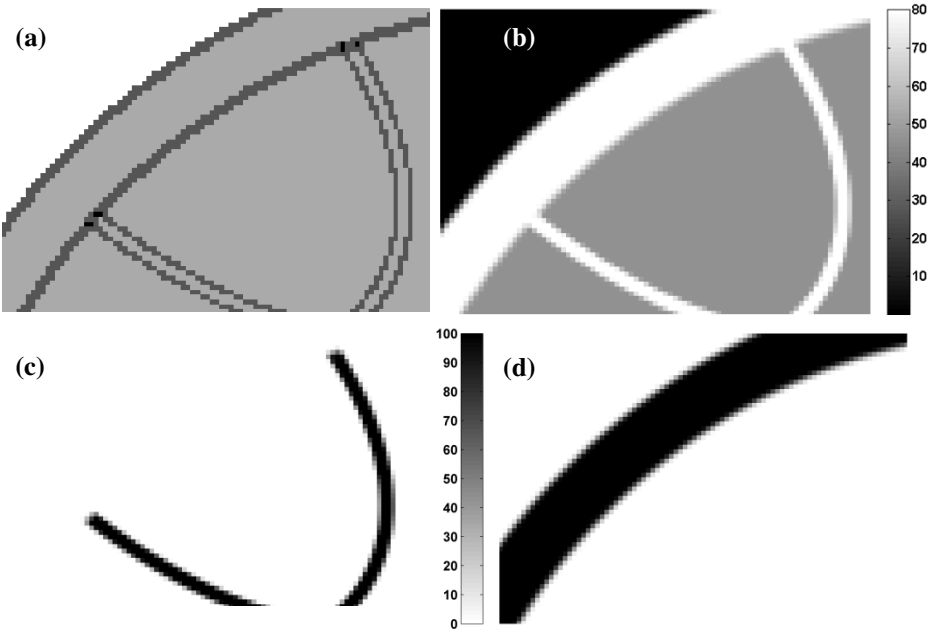

Fig. 5. Detail of a 450ml phantom with 400μm voxel size: (a) Segmentation of a phantom into air and voxels containing one (light gray), two (dark gray) or three (black) materials; (b) Simulated linear attenuation coefficients of voxels in (a) (in cm^{-1}, assuming monoenergetic x-ray beam at 20 keV); and percentage of (c) ligament tissue and (d) skin tissue in voxels from (a).

Fig. 6 shows simulated x-ray projections of phantoms with and without simulated PV. The simulated acquisition assumed a monoenergetic x-ray beam (at 20 keV) and parallel x-ray propagation, without scatter or quantum noise. The projections correspond to three phantoms with identical distributions of compartments: the phantom with 400μm voxels and no PV (Fig. 6a); the 400μm phantom with simulated PV (Fig. 6b); and the phantom with 200μm voxels and no PV (Fig. 6c). Shown also is the difference between the projections with and without simulated PV (Fig. 6d).

In a projection of the phantom with PV in Fig. 6b, the skin and Cooper's ligaments appear thinner (as compared to the phantom without PV, Fig. 6a). We believe this is caused by the reduction in the effective x-ray attenuations of voxels on the ligament/adipose tissue boundaries, which are lower than the x-ray attenuation of dense tissue (see Fig. 5b). Further, the characteristic stair-step quantization artifacts on tissue boundaries were noticeably reduced with simulated PV, as seen in the difference between PV and non PV projections (Fig 6d). Comparison of Figs. 6b and 6c indicates similar appearance of a phantom with PV simulated at a lower resolution (400μm) to a phantom simulated at a higher resolution (200μm) with no simulated PV. Hence, the application of PV may lead to an improvement in image quality without reducing voxel size.

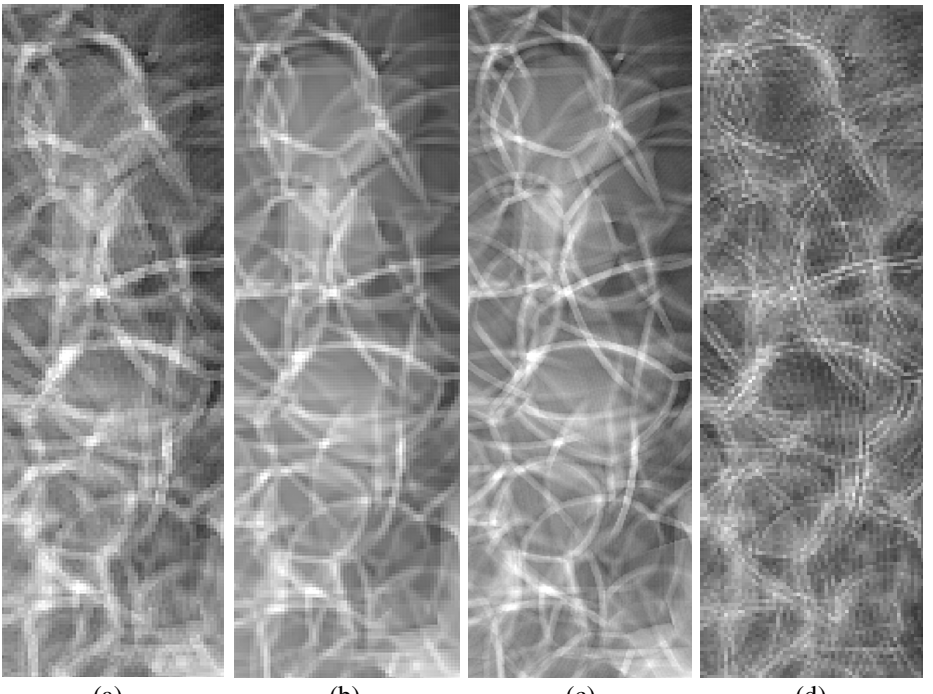

(a) (b) (c) (d)

Fig. 6. Simulated projections of (a) a phantom with 400μm voxels and no PV; (b) the phantom from (a) with simulated PV; and (c) the same phantom generated at 200 μm voxels and no PV. (d) The difference between (a) and (b); the image contrast was enhanced for display purposes.

4 Conclusion

We have developed and qualitatively assessed a method for PV simulation of phantom voxels containing up to three simulated materials. The percentage of simulated tissues was estimated based upon the use of the Gauss-Ostrogradsky theorem. Cross-section and projections of phantoms with and without PV simulation were visually compared. PV simulation can improve the quality of phantom images by reducing the quantization artifacts caused by large voxel sizes.

Acknowledgements. This work was supported in part by the US Department of Defense Breast Cancer Research Program (HBCU Partnership Training Award #BC083639), the US National Institutes of Health (R01 grant #CA154444), the US National Science Foundation (CREOSA grant #HRD-0630388), and the US Department of Defense/Department of Army (45395-MA-ISP, #54412-CI-ISP). The authors would like to thank Ms. Susan Ng from Real-Time Tomography (Villanova, PA) for processing the simulated projection images.

References

1. Pokrajac, D.D., Maidment, A.D.A., Bakic, P.R.: Optimized generation of high resolution breast anthropomorphic software phantoms. Medical Physics 39, 2290–2302 (2012)
2. Bakic, P.R., Zhang, C., Maidment, A.D.A.: Development and Characterization of an Anthropomorphic Breast Software Phantom Based upon Region-Growing Algorithm. Medical Physics 38, 3165–3176 (2011)
3. Bliznakova, K., Suryanarayanan, S., Karellas, A., Paiilikarakis, N.: Evaluation of an improved algorithm for producing realistic 3D breat software phantoms: Application for mammography. Medical Physics 37, 5604–5617 (2010)
4. Chen, B., Shorey, J., Saunders, R.S.J., Richard, S., Thompson, J., Nolte, L.W., Samei, E.: An anthropomorphic breast model for breast imaging simulation and optimization. Academic Radiology 18, 536–546 (2011)
5. O'Connor, J.M., Das, M., Didier, C., Mah'D, M., Glick, S.J.: Comparison of Two Methods to Develop Breast Models for Simulation of Breast Tomosynthesis and CT. In: Krupinski, E.A. (ed.) IWDM 2008. LNCS, vol. 5116, pp. 417–425. Springer, Heidelberg (2008)
6. Chen, F., Pokrajac, D.D., Shi, X., Liu, F., Maidment, A.D.A., Bakic, P.R.: Partial Volume Simulation in Software Breast Phantoms. In: Physics of Medical Imaging. SPIE, San Diego (2012)
7. Folland, G.B.: Advanced Calculus. Prentice-Hall, Inc., Upper Saddle River (2002)